Electric-Field Control of Magnetization, Jahn-Teller Distortion, and Orbital Ordering in Ferroelectric Ferromagnets

Lan Chen,[1,2,3] Changsong Xu,[1] Hao Tian,[2,3] Hongjun Xiang,[4,5] Jorge Íñiguez,[6,7] Yurong Yang,[1,2,3,5,*] and L. Bellaiche[1]

[1]*Physics Department and Institute for Nanoscience and Engineering, University of Arkansas, Fayetteville, Arkansas 72701, USA*
[2]*National Laboratory of Solid State Microstructures, Department of Materials Science and Engineering, Nanjing University, Nanjing 210093, China*
[3]*Jiangsu Key Laboratory of Artificial Functional Materials, Nanjing University, Nanjing 210093, China*
[4]*Key Laboratory of Computational Physical Sciences (Ministry of Education), State Key Laboratory of Surface Physics, and Department of Physics, Fudan University, Shanghai, 200433, China*
[5]*Collaborative Innovation Center of Advanced Microstructures, Nanjing 210093, China*
[6]*Materials Research and Technology Department, Luxembourg Institute of Science and Technology, 5 avenue des Hauts-Fourneaux, L-4362 Esch/Alzette, Luxembourg*
[7]*Physics and Materials Science Research Unit, University of Luxembourg, 41 Rue du Brill, L-4422 Belvaux, Luxembourg*

(Received 6 November 2018; revised manuscript received 19 April 2019; published 21 June 2019)

Controlling the direction of the magnetization by an electric field in multiferroics that are both ferroelectric and strongly ferromagnetic will open the door to the design of the next generation of spintronics and memory devices. Using first-principles simulations, we report that the discovery that the $PbTiO_3/LaTiO_3$ (PTO/LTO) superlattice possesses such highly desired control, as evidenced by the electric-field-induced rotation of 90° and even a possible full reversal of its magnetization in some cases. Moreover, such systems also exhibit Jahn-Teller distortions, as well as orbital orderings, that are switchable by the electric field, therefore making PTO/LTO of importance for the tuning of electronic properties too. The origin for such striking electric-field controls of magnetization, Jahn-Teller deformations, and orbital orderings resides in the existence of three different types of energetic coupling: one coupling polarization with antiphase and in-phase oxygen octahedral tiltings, a second one coupling polarization with antiphase oxygen octahedra tilting and Jahn-Teller distortions, and finally a biquadratic coupling between antiphase oxygen octahedral tilting and magnetization.

DOI: 10.1103/PhysRevLett.122.247701

Introduction.—Multiferroic materials hold promise for use in next-generation memory devices in which, e.g., the electric field controls magnetism [1,2]. Such materials are rare owing to a typical incompatibility between ferroelectricity and magnetism [3]. This incompatibility has provided motivation for an extensive search for new multiferroic materials [4–9] in which an electric-field control of magnetism was also investigated. For instance, the weak ferromagnetism and Dzyaloshinskii-Moriya (DM) vector in $BiFeO_3$ can be switched by 180° under an electric field by a two-step sequential rotation of the polarization [10]. Moreover, the weak ferromagnetism of hybrid improper ferroelectric superlattices, such as $BiFeO_3/NdFeO_3$ [11] and $BiFeO_3/LaFeO_3$ [12], and of Ruddlesden-Popper oxides with *B*-site cation ordered $A_3BB'O_7$ [13] was also predicted to be controllable by an electric field because the polarization is coupled with other nonpolar lattice distortions. However, all of the latter multiferroics possess a predominant antiferromagnetic alignment; that is, they "only" have weak ferromagnetism and/or are ferrimagnetic [14,15]. On the other hand, strong ferromagnetism has been found or predicted in $EuTiO_3$ [16], $BiMnO_3$ [17], La_2NiMnO_6/R_2NiMnO_6 [7], and $A^{2+}TiO_3/R^{3+}TiO_3$ [18] multiferroics, but electric-field control of such ferromagnetism has not been documented there. As a result, we are not aware that strong ferromagnetism has ever been reported to be controllable by an electric field in any single phase of any multiferroics.

Moreover, Jahn-Teller (JT) distortion [19] and orbital order (OO) [20] are common phenomena in oxides, and they are considered to be the origin of many physical behaviors. For instance, JT distortion and OO effects are intimately linked to electronic properties and lead to removing electronic degeneracy, opening band gaps, and affecting magnetic properties. Furthermore, JT distortion and OO effects play an important role in colossal magnetoresistance phenomena in manganites [21], superconductivity [22], polarization in perovskites [23,24], and strong electronic correlation [25]. It is also highly

desirable for functionality to tune JT distortions, OO, and corresponding electronic properties by an electric field. Note that Varignon and co-workers [24,26] showed that JT distortions can influence magnetic and orbital orderings, and suggested that the magnitude of JT distortions can be tuned by the electric field in some perovskites; however, the switchability of JT distortions and OO is unknown.

Here, by means of first-principles calculations, we investigate electrical, electronic, and magnetic properties of $PbTiO_3/LaTiO_3$ (PTO/LTO) superlattices as well as their change under an electric field. These simulations show that PTO/LTO superlattices are magnetoelectric ferroelectrics, similar to those in Ref. [18], and they possess a strong magnetization that can be switched by 90° under an electric field that is perpendicular to the initial polarization—consequently leading to a possible electric-field-induced reversal of ferromagnetism via a two-step process. This control of magnetization originates from a biquadratic energetic coupling between magnetization and antiphase oxygen octahedral rotations, with the latter quantities also being coupled with polarization via trilinear couplings. We additionally found that an electric field can also switch the JT and OO vectors when the electric field is antiparallel to the initial direction of the polarization. These new phenomena for controlling strong ferromagnetism, Jahn-Teller distortion and orbital ordering, provide a new avenue to tune magnetic and electronic properties, in particular, and functionality, in general, in perovskites.

Structural, electronic, and magnetic properties.—Density-functional calculations were performed on PTO/LTO superlattices. Technically, $[PTO]_1/[LTO]_1$ superlattices are investigated here, for which one unit layer of $PbTiO_3$ successively alternates with one unit layer of $LaTiO_3$ along the pseudocubic [001] direction. Structures, electric, and magnetic properties without applying an electric field and under an electric field are investigated. More details about the method are given in the Supplemental Material [27]. $PbTiO_3$ bulk possesses a tetragonal polar ground state (space group $P4mm$) with a polarization pointing along **c**. On the other hand, the ground state of $LaTiO_3$ is an orthorhombic nonpolar phase (space group $Pbnm$) with an in-plane antiphase oxygen octahedral tilting and an out-of-plane in-phase oxygen octahedral tilting [which constitute antiferrodistortive (AFD) motions having the $a^-a^-c^+$ pattern in Glazer's notation [37]]. We numerically found that the PTO/LTO superlattice adopts a monoclinic phase (space group $P2_1$) with a similar $a^-a^-c^+$ AFD pattern as LTO. The lattice constants of this superlattice ($a = 5.58$ Å, $b = 5.63$ Å, and $c = 7.91$ Å) are close to the averages of those of cubic PTO ($a_1\sqrt{2} = 5.56$ Å, $a_2\sqrt{2} = 5.56$ Å, and $2a_3 = 7.86$ Å) and LTO ($a = 5.61$ Å, $b = 5.71$ Å, and $c = 7.87$ Å) bulks. Note that the predicted lattice constants of PTO and LTO agree rather well with the experiments (the difference is less than 1.5%) [38,39].

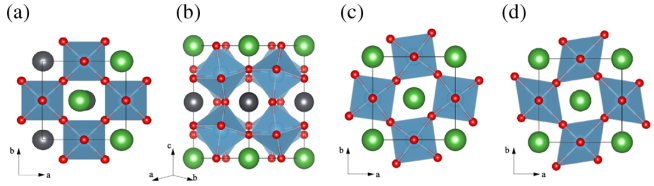

FIG. 1. Geometry and major structural distortions of the ground state of the studied PTO/LTO superlattice. (a) Polarization distortion P about the in-plane **a** axis ([−110] direction). (b) Antiphase oxygen octahedral rotations Φ_{xy} about the in-plane **a** axis ([110] direction). (c) In-phase oxygen octahedral rotations Θ_z about the out-of-plane **c** axis ([001] direction). (d) Q Jahn-Teller lattice distortion.

We further found that the charge order between Ti^{4+} in PTO and Ti^{3+} in LTO induces striking structural features and electronic properties in the PTO/LTO superlattice. More precisely, there are two Ti d^1 and two Ti d^0 ions in our supercell, with these two types of Ti ions being arranged in a rocksalt configuration within the B sublattice. In other words, the nearest neighbors of Ti d^1 ions in the B sublattice are Ti d^0 ions, and vice versa. This d^1-d^0 charge ordering generates a breathing distortion of oxygen octahedral cages (B_{OC}), for which the Ti^{3+} d^1 orbital occupation expands the corresponding oxygen octahedral cage, while the Ti^{4+} d^0 orbital occupation shrinks the corresponding oxygen octahedral cage. Note that, in order to investigate the orbitals of Ti ions in details, we studied the projected density of states on Ti ions. We found that the Ti^{4+} ions have an almost empty d orbital, while the Ti^{3+} ions display a mixed $d_{xy} + d_{xz}$ or $d_{xy} + d_{yz}$ character. The latter strong hybridizations of two d orbitals lead to an insulating character in the PTO/LTO system, similar to the case of ferromagnetic $A^{2+}TiO_3/R^{3+}TiO_3$ superlattices (A = Sr, Ca, Ba; R = Sm, Y, Tm, La, Pr, Lu) [18], in which similar charge and orbital orderings are found. As a matter of fact, these hybridizations of two orbitals $d_{xy} + d_{xz}$ or $d_{xy} + d_{yz}$ result in the presently considered system being ferromagnetic semiconductor on the basis of intrasite Hund's rules [18]. Practically, the computed band gap is 0.5 eV and the energy of the ferromagnetic configuration is lower than that of the A-type antiferromagnetic configuration by 10 meV per Ti^{3+} ion. Moreover, from our noncollinear magnetic configuration calculations, the PTO/LTO system has mainly ferromagnetism lying along the in-plane **b** direction with a magnetic moment of about $0.99\mu_B$ per Ti^{3+} accompanied by a weak ferromagnetism being along the out-of-plane **c** direction and of about $0.03\mu_B$ magnitude per supercell. The PTO/LTO superlattice has also a polarization oriented along the **−a** direction with a magnitude of 16.9 $\mu C/cm^2$, which has the character of hybrid-improper ferroelectricity, as discussed below [7,40].

Moreover, the $P2_1$ ground state of PTO/LTO consists of a combination of several lattice distortions of the

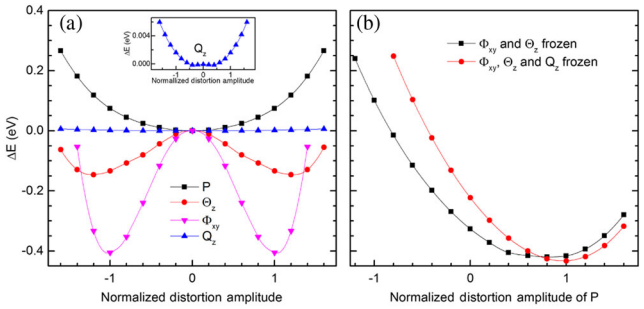

FIG. 2. Dependence on the total energy on amplitude of distortion in the investigated PTO/LTO superlattice. (a) Energy with respect to the amplitude of the main four lattice distortions, P, Φ_{xy}, Θ_z, and Q_z. (b) Energies as a function of amplitude of P when fixing Φ_{xy} and Θ_z (black squares), as well as those when fixing Φ_{xy}, Θ_z, and Q_z (red circles), to their values in the ground state.

high-symmetry ($P4/mmm$) double perovskite. Such a ground state possesses four main phonon modes having large magnitude: (1) a ferrilike polar A-cation motions [41], where Pb and La ions move in opposite direction and with different amplitude, which results in a polar mode (P), as depicted in Fig. 1(a) [11]; (2) an antiphase tilting of oxygen octahedra about the a axis [Φ_{xy}; see Fig. 1(b)]; (3) an in-phase tilting about the c axis [Θ_z; see Fig. 1(c)]; and (4) the B_{OC} breathing motion that is related to the charge order between Ti^{4+} and Ti^{3+} ions and that expands or contracts oxygen octahedra. In the ground state of PTO/LTO superlattice, there is another mode, which is of a Jahn-Teller nature [Q_z; see Fig. 1(d)] and which has an amplitude much smaller than the other four aforementioned modes, but the Jahn-Teller mode plays a key role in electronic properties and may couple to polarization and other distortion modes.

We then perform an energy expansion in terms of these lattice distortions and identify the following couplings [18,26,42–44]:

$$\mathcal{F} \propto P_x\Phi_x\Theta_z, P_y\Phi_y\Theta_z, P_x\Phi_xQ_z, P_y\Phi_yQ_z, \qquad (1)$$

where the x, y, and z subscripts refer to Cartesian components along the corresponding axis.

We project out the contribution of each Φ, Θ, Q, and P modes to the $P2_1$ ground state structure and calculate the energy surface around the $P4/mmm$ reference structure by individually condensing each mode. Figure 2(a) displays the resulting total energy as a function of the amplitude of each distortion for these four modes. One can clearly see that the P mode, by itself, is stable, whereas large energy gains occur for Φ_{xy} and Θ_z—resulting in characteristic double-well potentials. Though the potential surface of Q_z is very flat with the magnitude of this mode, the inset of Fig. 2(a) indicates that the Q_z mode in $P4/mmm$ structure is barely unstable. The black squares (red circles) in Fig. 2(b) display the total energy of the state as a function of the amplitude of P, but with freezing Φ_{xy} and Θ_z (Φ_{xy}, Θ_z, and Q_z) distortions to those of the ground state. In contrast to the single minimum of P at $P = 0$ in Fig. 2(a), when the other modes are null, polarization in Fig. 2(b) becomes unstable and its minimum shifts to a nonzero value. The resulting energy gain when freezing Φ_{xy}, Θ_z, and Q_z is more than that obtained when freezing only Φ_{xy} and Θ_z. The energy as a function of amplitude of P when freezing Φ_{xy} and Q_z (not shown here) also exhibits a single well, similar to that shown in Fig. 2(b), but with smaller energy gain. These features are direct indications that trilinear couplings $P\Phi\Theta$ and $P\Phi Q$ of Eq. (1) are both in play here. These trilinear couplings lead to a polarization of 16.9 $\mu C/cm^2$.

Properties under an electric field.—These observations of two types of trilinear couplings between P, Φ, Θ, and Q also suggest that the switching of polarization by an electric field may induce the switching of Φ, or the switching of both Θ and Q. We first consider the case of switching the polarization by 90°, by applying an electric field along $-\mathbf{b}$ that is perpendicular to the initial polarization lying along $-\mathbf{a}$. Figure 3(a) represents the energy difference ($\Delta E_{\mathrm{FM}_a-\mathrm{FM}_b}$) between the ferromagnetic spin configurations along $\mathbf{a}$ and $\mathbf{b}$, as well as the polarization (P) and AFD angles (Φ, Θ) as a function of this applied electric field. Under an electric field ranging from 0 to 0.062 V/Å, the $\mathbf{a}$ component of the polarization keeps a value of about -16 $\mu C/cm^2$, while its $\mathbf{b}$ component increases in magnitude from about zero to -33 $\mu C/cm^2$. Under this electric field range of 0–0.062 V/Å, the AFD (antiphase) angles Φ_x and Φ_y both keep a value of about 7° and the AFD (in-phase) Θ_z remains at about −7.4°. The magnetic easy axis is along $\mathbf{b}$ or $-\mathbf{b}$ (the two opposite directions are symmetrically equivalent), as indicated by the energy difference shown in top panel of Fig. 3(a). At an electric field of 0.063 V/Å, the polarization P, the in-plane antiphase oxygen octahedra tilting Φ, and the magnetic easy axis are all switched by 90° with respect to the case under no field. More precisely, polarization is switched to $-\mathbf{b}$, Φ_x is reversed from 7° to −7° (resulting in the axis of rotation of the antiphase tilting switching from $\mathbf{a}$ to $\mathbf{b}$), and the magnetic easy axis is now aligned along $\mathbf{a}$. When the electric field along $\mathbf{b}$ further increases to 0.085 V/Å, the polarization further increases in magnitude from 71 to 79 $\mu C/cm^2$, while the x, y, and z components of the AFD tilting are now about −6.5°, 6.2°, and −7°, respectively. Meanwhile, the $\Delta E_{\mathrm{FM}_a-\mathrm{FM}_b}$ energy difference between the magnetic easy axes $\mathbf{a}$ and $\mathbf{b}$ is always negative, and its magnitude slightly increases when the electric field increases, therefore stabilizing even more an easy magnetic axis along $\mathbf{a}$.

Furthermore, when the electric field is released [see the black open symbols in Fig. 3(a)], P, Φ_y, Θ, and $\Delta E_{\mathrm{FM}_a-\mathrm{FM}_b}$ do not change their signs. In other words, after removal

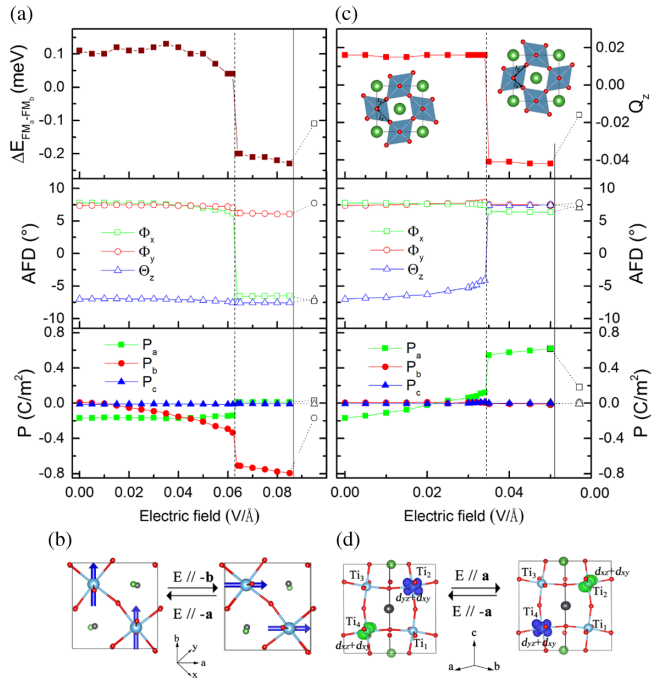

FIG. 3. (a),(b) Physical quantities as a function of the electric field applied along $-\mathbf{b}$, i.e., perpendicular to the initial direction of the polarization, and (c),(d) applied along $\mathbf{a}$, i.e., antiparallel to the initial direction of the polarization, in the studied PTO/LTO superlattice. (a) Energy difference between ferromagnetic configurations along $\mathbf{a}$ and $\mathbf{b}$; oxygen octahedral tilting angles, Φ_x, Φ_y, and Θ_z; and polarization $\mathbf{P}$. (b) Schematization of the spin configurations on Ti^{3+} ions, which can be switched by 90° via the application of electric fields oriented along the $-\mathbf{b}$ axis or the $-\mathbf{a}$ axis. (c) JT distortion Q, and oxygen octahedral tilting angles and polarization. (d) Charge density of states near the Fermi level in energy range from −0.5 to 0 eV. The black open symbols in (a) and (c) represent the same quantities when the electric field is released.

of a large enough electric field, P, Φ, and the magnetic easy axis all undergo a switching by 90° with respect to the initial zero-field state. These promising switching of strong ferromagnetism shown in Fig. 3(a) have never been found in any material [10–13,45].

It is known, from the knowledge of magnetic space group and group theory [12], that antiphase oxygen octahedral rotation controls the orientation of the magnetization. To better understand the mechanism of the aforementioned switching of strong ferromagnetism, we also determined couplings between AFD and magnetism order parameters, which are found to be of the form

$$\mathcal{F} \propto \Phi_x \Phi_y M_x M_y, \tag{2}$$

where Φ_x, Φ_y are antiphase oxygen octahedra tiltings along the pseudocubic [100] and [010] directions, respectively, while M_x and M_y are the components of the magnetization along the [100] and [010] directions, respectively. The ground state of Fig. 3(a) under zero electric field possesses a magnetic moment given by $M_x = -1.41\mu_B$ and $M_y = 1.41\mu_B$ per 20 atoms (which is therefore mostly along the $\mathbf{b}$ orthorhombic axis), and an antiphase tilting quantified by $\Phi_x = 7°$ and $\Phi_y = 7°$. We found that this phase transforms, under the application of an aforementioned large enough electric field applied along $-\mathbf{b}$, followed by a removal of such field, to another energetically degenerate phase having a magnetic moment given by $M_x = M_y = 1.41\mu_B$ (which is mostly along $\mathbf{a}$), and an antiphase tilting given by $\Phi_x = -7°$ and $\Phi_y = 7°$. According to Eq. (2), such a change of sign of M_x originates from the electric-field-induced reversal of Φ_x.

We thus found that a large enough electric field applied perpendicularly to the initial direction of the polarization can transform PTO/LTO from adopting a phase I [M_b,Φ_a, P_{-a}] to another phase II [M_a, Φ_b, P_{-b}]. As schematized in Fig. 3(b), applying an electric field along $-\mathbf{a}$ to this phase II should then make the system come back either to its initial phase I [M_b, Φ_a, P_{-a}] or to another phase with [M_{-b},Φ_a, P_{-a}] since changing the magnetization from M_b to M_{-b} has no effect on the biquadratic energy of Eq. (2). Moreover, following Eqs. (1) and (2) also implies that applying now an electric field along $\mathbf{a}$ to this phase II [M_a, Φ_b, P_{-b}] should then transform it into a phase III characterized by [M_{-b}, Φ_{-a}, P_a] or into a phase IV for which [M_b, Φ_{-a}, P_a]. As a result, this two-step process opens the door to reversing a strong ferromagnetic moment by application of electric fields, which is a possibility unheard of. Yet, from our calculations, we can say only that the switch has only a 50% chance to occur.

We next consider the situation of applying electric fields to phase I along the opposite direction of its polarization (that is, we apply an electric field along $+\mathbf{a}$). Under such electric fields with a magnitude ranging from zero to 0.034 V/Å and as shown in Fig. 3(c), the polarization smoothly changes its $\mathbf{a}$ component from (negative) $-17\ \mu C/cm^2$ to (positive) $+12\ \mu C/cm^2$, while the antiphase in-plane tilting Φ_x and Φ_y keep almost the same value of 7.5° and the out-of-plane in-phase tilting reduces its value from −7° to −4.1°. To better describe the Jahn-Teller distortion of oxygen octahedra, we define its Q_z order parameter as the length difference between the Ti—O bond along the $\mathbf{x}$ axis [called l_x in the inset of Fig. 3(c)] and the Ti—O bond along the $\mathbf{y}$ axis [denoted as l_y in the inset of Fig. 3(c) and belonging to the same oxygen octahedron as l_x]. Negative Q_z corresponds to shrinking in the $\mathbf{x}$ direction and expansion in the $\mathbf{y}$ direction, while positive Q_z implies expansion along $\mathbf{x}$ and shrinking along $\mathbf{y}$. From Fig. 3(c), one can see that oxygen octahedra slightly expand in the $\mathbf{x}$ direction under such electric field varying from zero to 0.034 V/Å. At a field of 0.035 V/Å, the polarization suddenly jumps from 12 to 54 $\mu C/cm^2$, the oxygen octahedral in-phase tilting Θ_z switches from −4.1° to +6.4°, and Q_z changes from about 0.02 to −0.04 Å. The polarization P,

in-phase tilting Θ, and JT distortion Q_z therefore all revert their directions with respect to the case of null field. Under a larger electric field, P, Φ, Θ, and JT distortion nearly retain their values associated with the 0.035 V/Å field. We also found that, when removing these large fields [see Fig. 3(c)], P, Θ, and JT distortion Q do not have a change of direction (while their magnitude can be modified). In other words, JT patterns can be reverted by applying and then removing a large enough electric field to a PTO/LTO superlattice [the inset of Fig. 3(c) schematizes the two JT distortion patterns that are switchable by such electric fields] [19,46].

Furthermore, Fig. 3(d) depicts the corresponding charge density of orbitals in the two phases which are switchable by an electric field parallel (or antiparallel) to **a**. The four Ti ions of our supercell are denoted by Ti_1, Ti_2, Ti_3, and Ti_4. Ti_1 and Ti_3 are +4 ions with essentially empty d shells, while Ti_2 and Ti_4 are +3 ions with one electron in d shell (also see Fig. S3 in the Supplemental Material [27]). In the left panel of Fig. 3(d) (which corresponds to the initial zero-field ground state), the main orbitals on Ti_2 are $d_{yz} + d_{xy}$ versus $d_{xz} + d_{xy}$ for Ti_4. When the JT distortion is reverted and is as displayed in Fig. 3(d), the main orbitals are now $d_{xz} + d_{xy}$ on Ti_2, and $d_{yz} + d_{xy}$ on Ti_4. The d_{yz} and d_{xz} orbitals are therefore switched between Ti_2 and Ti_4 under such an electric field. A change of Jahn-Teller distortion patterns [see the inset of Fig. 3(c)] leads to a specific change of the corresponding orbitals ($d_{xz} + d_{xy}$ versus $d_{yz} + d_{xy}$ for that specific Ti^{3+} ion). Consequently, switching the Jahn-Teller pattern by an electric field [as a result of a trilinear coupling indicated in Eq. (1)] subsequently results in the switching of orbital ordering. Such an orbital effect may provide us a new way to modulate electronic structure and thus affect magnetism, superconductivity, topological properties, etc. [24,26].

In summary, we demonstrated electronic control of strong ferromagnetism, JT distortion, and orbital ordering in the multiferroic PTO/LTO superlattice. Interestingly, the lattice parameters of PTO/LTO ($a = 5.58$ Å, $b = 5.63$ Å) are close (namely, less than 1%) to those of commercial substrates such as $DyScO_3$, $TbScO_3$, $GdScO_3$, $SmScO_3$, $NdScO_3$, and $PrScO_3$. Growing epitaxial PTO/LTO films on these substrates, via, e.g., pulsed laser deposition and molecular beam epitaxy techniques, should thus be practically achievable. Note also that $A^{2+}TiO_3/R^{3+}TiO_3$ superlattices (A = Sr, Ca, Ba; R = Sm, Y, Tm, La, Pr, Lu) have similar ferroelectric and ferromagnetic properties to our PTO/LTO studied system [18]. We thus expect that the presently determined electrically induced switching of ferromagnetism, JT distortions, and orbital ordering should also be realizable in $A^{2+}TiO_3/R^{3+}TiO_3$ superlattices.

Y. Y. and L. B. was supported by ONR Grant No. N00014-17-1-2818. C. X. acknowledges the U.S. DOE, Office of Basic Energy Sciences, for Award No. DE-SC0002220. L. B. and J. I. were also supported by Luxembourg National Research Fund Grant No. INTER/MOBILITY/15/9890527 (GREENOX). L. C, H. T., and Y. Y. also acknowledge the state key program for basic research of China (Contract No. 2015CB921203) and NSFC (Contract No. 11874207).

*yangyr@nju.edu.cn

[1] N. A. Spaldin and M. Fiebig, Science **309**, 391 (2005).
[2] W. Eerenstein, N. Mathur, and J. F. Scott, Nature (London) **442**, 759 (2006).
[3] N. A. Hill, J. Phys. Chem. B **104**, 6694 (2000).
[4] T. Kimura, T. Goto, H. Shintani, K. Ishizaka, T.-h. Arima, and Y. Tokura, Nature (London) **426**, 55 (2003).
[5] J. Wang, J. Neaton, H. Zheng, V. Nagarajan, S. Ogale, B. Liu, D. Viehland, V. Vaithyanathan, D. Schlom, U. Waghmare *et al.*, Science **299**, 1719 (2003).
[6] A. Kumar, R. Katiyar, R. N. Premnath, C. Rinaldi, and J. Scott, J. Mater. Sci. **44**, 5113 (2009).
[7] H. J. Zhao, W. Ren, Y. Yang, J. Íñiguez, X. M. Chen, and L. Bellaiche, Nat. Commun. **5**, 4021 (2014).
[8] M. J. Pitcher, P. Mandal, M. S. Dyer, J. Alaria, P. Borisov, H. Niu, J. B. Claridge, and M. J. Rosseinsky, Science **347**, 420 (2015).
[9] M. Kenzelmann, A. B. Harris, S. Jonas, C. Broholm, J. Schefer, S. B. Kim, C. L. Zhang, S.-W. Cheong, O. P. Vajk, and J. W. Lynn, Phys. Rev. Lett. **95**, 087206 (2005).
[10] J. Heron, J. Bosse, Q. He, Y. Gao, M. Trassin, L. Ye, J. Clarkson, C. Wang, J. Liu, S. Salahuddin *et al.*, Nature (London) **516**, 370 (2014).
[11] B. Xu, D. Wang, H. J. Zhao, J. Íñiguez, X. M. Chen, and L. Bellaiche, Adv. Funct. Mater. **25**, 3626 (2015).
[12] Z. Zanolli, J. C. Wojdeł, J. Íñiguez, and P. Ghosez, Phys. Rev. B **88**, 060102(R) (2013).
[13] X.-Z. Lu and J. M. Rondinelli, Adv. Funct. Mater. **27**, 1604312 (2017).
[14] H. Das, A. L. Wysocki, Y. Geng, W. Wu, and C. J. Fennie, Nat. Commun. **5**, 2998 (2014).
[15] J. A. Mundy, C. M. Brooks, M. E. Holtz, J. A. Moyer, H. Das, A. F. Rébola, J. T. Heron, J. D. Clarkson, S. M. Disseler, Z. Liu *et al.*, Nature (London) **537**, 523 (2016).
[16] J. H. Lee, L. Fang, E. Vlahos, X. Ke, Y. W. Jung, L. F. Kourkoutis, J.-W. Kim, P. J. Ryan, T. Heeg, M. Roeckerath *et al.*, Nature (London) **466**, 954 (2010).
[17] M. Gajek, M. Bibes, A. Barthélémy, K. Bouzehouane, S. Fusil, M. Varela, J. Fontcuberta, and A. Fert, Phys. Rev. B **72**, 020406(R) (2005).
[18] N. Bristowe, J. Varignon, D. Fontaine, E. Bousquet, and P. Ghosez, Nat. Commun. **6**, 6677 (2015).
[19] J. B. Goodenough, Annu. Rev. Mater. Sci. **28**, 1 (1998).
[20] A. I. Liechtenstein, V. I. Anisimov, and J. Zaanen, Phys. Rev. B **52**, R5467 (1995).
[21] B. Raveau, M. Hervieu, A. Maignan, and C. Martin, J. Mater. Chem. **11**, 29 (2001).
[22] J. G. Bednorz and K. A. Müller, Rev. Mod. Phys. **60**, 585 (1988).
[23] C. Xu, Y. Li, B. Xu, J. Íñiguez, W. Duan, and L. Bellaiche, Adv. Funct. Mater. **27**, 1604513 (2017).

[24] J. Varignon, N. C. Bristowe, and P. Ghosez, Phys. Rev. Lett. **116**, 057602 (2016).
[25] R. Berthelot, D. Carlier, and C. Delmas, Nat. Mater. **10**, 74 (2011).
[26] J. Varignon, N. C. Bristowe, E. Bousquet, and P. Ghosez, Sci. Rep. **5**, 15364 (2015).
[27] See Supplemental Material at http://link.aps.org/supplemental/10.1103/PhysRevLett.122.247701, which includes Refs. [28–36] and discuss the details in computations, free energy expansion, effect of strain, and orbital ordering change under electric field.
[28] J. P. Perdew, A. Ruzsinszky, G. I. Csonka, O. A. Vydrov, G. E. Scuseria, L. A. Constantin, X. Zhou, and K. Burke, Phys. Rev. Lett. **100**, 136406 (2008).
[29] G. Kresse and D. Joubert, Phys. Rev. B **59**, 1758 (1999).
[30] J. Heyd, G. E. Scuseria, and M. Ernzerhof, J. Chem. Phys. **118**, 8207 (2003).
[31] R. D. King-Smith and D. Vanderbilt, Phys. Rev. B **47**, 1651 (1993).
[32] H. Fu and L. Bellaiche, Phys. Rev. Lett. **91**, 057601 (2003).
[33] L. Chen, Y. Yang, and X. Meng, Sci. Rep. **6**, 25346 (2016).
[34] B. Xu, J. Íñiguez, and L. Bellaiche, Nat. Commun. **8**, 15682 (2017).
[35] Z. Jiang, Y. Nahas, S. Prokhorenko, S. Prosandeev, D. Wang, J. Íñiguez, and L. Bellaiche, Phys. Rev. B **97**, 104110 (2018).
[36] P. Chen, R. J. Sichel-Tissot, J. Young Jo, R. T. Smith, S.-H. Baek, W. Saenrang, C.-B. Eom, O. Sakata, E. M. Dufresne, and P. G. Evans, Appl. Phys. Lett. **100**, 062906 (2012).
[37] A. Glazer, Acta Crystallogr. Sect. B **28**, 3384 (1972).
[38] O. Yamaguchi, A. Narai, T. Komatsu, and K. Shimizu, J. Am. Ceram. Soc. **69**, C-256 (1986).
[39] M. Eitel and J. Greedan, J. Less-Common Met. **116**, 95 (1986).
[40] N. A. Benedek and C. J. Fennie, Phys. Rev. Lett. **106**, 107204 (2011).
[41] A. T. Mulder, N. A. Benedek, J. M. Rondinelli, and C. J. Fennie, Adv. Funct. Mater. **23**, 4810 (2013).
[42] T. Fukushima, A. Stroppa, S. Picozzi, and J. M. Perez-Mato, Phys. Chem. Chem. Phys. **13**, 12186 (2011).
[43] J. M. Rondinelli and C. J. Fennie, Adv. Mater. **24**, 1961 (2012).
[44] N. Miao, N. C. Bristowe, B. Xu, M. J. Verstraete, and P. Ghosez, J. Phys. Condens. Matter **26**, 035401 (2014).
[45] P. S. Wang, W. Ren, L. Bellaiche, and H. J. Xiang, Phys. Rev. Lett. **114**, 147204 (2015).
[46] H. Köppel, D. R. Yarkony, and H. Barentzen, *The Jahn-Teller Effect* (Springer, New York, 2007).